Anodic TiO2 Nanotube Layers for Wastewater and Air Treatments: Assessment of Performance Using Sulfamethoxazole Degradation and N2O Reduction

Marcel Sihor, Sridhar Gowrisankaran, Alexandr Martaus, Martin Motola, Gilles Mailhot, Marcello Brigante, Olivier Monfort

molecules

MDPI

Article

Anodic TiO_2 nanotube layers for wastewater and air treatments: Assessment of performance using sulfamethoxazole degradation and N_2O reduction

Marcel Sihor [1,2], Sridhar Gowrisankaran [1], Alexandr Martaus [2], Martin Motola [1], Gilles Mailhot [3], Marcello Brigante [3] and Olivier Monfort [1,*]

[1] Department of Inorganic Chemistry, Faculty of Natural Sciences, Comenius University Bratislava, Ilkovicova 6, Mlynska Dolina, 84215 Bratislava, Slovakia
[2] Institute of Environmental Technology, CEET, VSB-Technical University of Ostrava, 17. Listopadu 15/2172; 70800, Ostrava-Poruba, Czech republic
[3] Institut de Chimie de Clermont-Ferrand, Université Clermont Auvergne, CNRS, Clermont Auvergne INP, F-63000 Clermont-Ferrand, France
* Correspondence: monfort1@uniba.sk; Tel.: +421290142141

Abstract: The preparation of anodic TiO_2 nanotube layers have performed using electrochemical anodization of Ti foil for 4 h at different voltages (from 0 V to 80 V). In addition, TiO_2 thin layer has been also prepared using the sol-gel method. All the photocatalysts has been characterized by XRD, SEM, and DRS to investigate the crystalline phase composition, the surface morphology and the optical properties, respectively. The performance of the photocatalyst has been assessed in versatile photocatalytic reactions including the reduction of N_2O gas and the oxidation of aqueous sulfamethoxazole. Due to their high specific surface area and excellent charge carriers transport, anodic TiO_2 nanotube layers have exhibited the highest N_2O conversion rate (up to 10% after 22 h) and the highest degradation extent of sulfamethoxazole (about 65% after 4 h) under UVA light. The degradation mechanism of sulfamethoxazole has been investigated by analyzing its transformation products by LC-MS and predominant role of hydroxyl radicals has been confirmed. Finally, the efficiency of anodic TiO_2 nanotube layer has been tested in real wastewater reaching up to 45% of sulfamethoxazole degradation after 4 h.

Keywords: photocatalysis; pharmaceutical; water treatment; air treatment; N_2O; TiO_2.

Citation: To be added by editorial staff during production.

Academic Editor: Firstname Lastname

Received: date
Accepted: date
Published: date

1. Introduction

With regard to number of publications, titania (TiO_2) is the most investigated photocatalyst in a multitude of applications such as, for example, antibacterial coatings and water and air treatments [1–6]. Efficient TiO_2 photocatalysts are prepared in the form of nanomaterials ranging from 0D to 3D morphologies [5,7–12]. The 1D titania nanostructures include TiO_2 nanotubes (TNT) and are promising nanostructured photocatalysts mainly due to their excellent electron transport [13–15]. In the form of self-organized arrays (i.e., supported layers), TNT exhibit enhanced charge carriers separation, thus leading to exceptional photocatalytic properties [13–16]. The preparation TNT layers can be done by anodic oxidation of Ti electrode in fluoride-containing electrolyte [17–19]. The variation of applied voltage and fluoride concentration and anodization time can be tuned to design TNT of specific length and wall thickness [17–20]. In addition, by extending one of these experimental parameters, the TNT morphology can be transformed in a porous nanostructure which exhibits also interesting photocatalytic properties as reported in our recent work [20].

The treatment of water by photocatalysis is one of the most investigated alternatives

to enhance the already existing processes which are used in wastewater treatment plants (WWTPs) and in the production of drinking water [21]. Indeed, photocatalytic process belongs to advanced oxidation processes (AOPs), thus generating reactive oxygen species (ROS) like hydroxyl radicals (HO•) [22]. The HO• react with high kinetic rate and non-selectively with organic molecules including persistent organic pollutants (POPs) and contaminants of emerging concern (CECs) [22]. Among CECs, pharmaceutical and personal care products (PPCPs) are daily consumed and their long-term impact on the natural environmental and the human health is not yet clarified [23,24]. Intergovernmental agencies have implemented stringent norms for pollution control and water quality, like the implementing decision of the European Union (EU) No. 2020/1161 on the directive No. 2008/105/CE [25]. Therefore, the modification of conventional water treatments appears a necessary conditions to fulfill these norms, thus TNT photocatalysts being excellent candidate. In this study, sulfamethoxazole (SMX) is used as a model pollutant since it is a widely used antibiotics. In addition, SMX is one of the most frequently detected pollutants in water around the World [23].

The treatment of air for the removal of nitrous oxide (N_2O) using photocatalytic reactions has been described back in the 1990s, when the first experiments employed zeolite containing Cu-based photocatalysts [26]. N_2O is in the top 3 gases responsible for the global warming since it has been proven to be involved at 6.2% of the total global radiative forcing. The major origin of N_2O is from natural processes (nitrification of ammonia, denitrification of nitrates, etc.) but also anthropogenic activities (N-based fertilizers, combustion of fossil fuels, etc.) [27]. Therefore, intense research is carrying out to develop different types of photocatalysts including TiO_2 [28–33]. However, one significant disadvantage of these already existing photocatalysts is that they are not easy to handle because of their powder form. Using supported TNT photocatalysts, such a drawback might be overcome.

In the present work, the use of anodic TNT layers in wastewater and air treatments is assessed using the degradation of aqueous sulfamethoxazole solution and the reduction of gaseous nitrous oxide, respectively, as model reactions. To the best of our knowledge, it is the first time that TNT layers are used in such versatile photocatalytic reactions, and their performance is compared to another TiO_2 nanostructure i.e. TiO_2 thin layer deposited by the sol-gel method. In addition, the degradation of SMX is also performed in real wastewater while the degradation pathway of SMX is proposed to clarify the mechanism.

2. Materials and Methods

2.1 Preparation and characterization of photocatalysts

The TNT layers are prepared using a similar procedure reported in one of our previous works [34]. Briefly, a disk of 4 cm in diameter of titanium foil (Sigma-Aldrich, 99.7 % with 0.127 mm thickness) is used as a working electrode and dropped in fluoride-based electrolyte based on glycerol. The counter electrode is also a 4 cm diameter Ti foil. The distance between the two electrodes is set at 1.5 cm and electrochemical anodization is performed at different applied voltages from 0 to 80 V (with a 20 V step) for 100 min. The current intensity is kept at 5 A during the procedure. After rinsing the as-prepared TNT followed by annealing at 400 °C for 1h, TNT layers labelled F0, F20, F40, F60 and F80 are obtained.

For comparison, TiO_2 sol-gel films are prepared. To this end, titanium isopropoxide (97.0%; Sigma-Aldrich) is added to isopropanol (reagent grade, Slavus sro.) containing acetic acid (99.0%, Slavus sro.) and Triton® X-100 (Sigma-Aldrich) as chelating and structure directing agents, respectively, thus a 0.2 M Ti alkoxide sol-gel is obtained. The sol-gel is deposited by spin-coating (Ossila Ltd.) at 2000 rpm on Si wafer (University Wafer Inc.) with diameter of 4 cm. Six-layer films are prepared with intermediate an-

nealing at 300 °C for 10 min and final annealing at 450 °C for 1 h. The TiO_2 sol-gel films are labelled SG.

The TNT and sol-gel layers are characterized by DRS (Shimadzu UV-2600, IRS-2600Plus), XRD (Rigaku SmartLab) and SEM (Tescan Lyra 3) to control the optical energy band gap (E_g), the crystalline phase composition and the surface morphology, respectively. Further characterization details of these reproducible nanomaterials are provided in our previous publications [20,34].

2.2 Degradation of N_2O in the gas phase

The photocatalytic decomposition of gaseous N_2O is performed in a custom-made stainless-steel photo-reactor (Figure 1) where the photocatalytic layer is placed at the bottom. After that, the reactor is closed and filled with N_2O/He mixture and pressurized to 1.5 bar (pressure is controlled during the whole experiment). The initial N_2O concentration is set at 1030 ppm. The irradiation is generated by UVA source (UVP Pen-Ray, 8 W Hg lamp; λ_{max} = 365 nm) situated at the top of photo-reactor and going through the quartz glass visor. The N_2O concentration is measured using a GC/BID (Gas Chromatography coupled with Barrier discharge Ionization detector, Shimadzu Tracera GC 2010Plus) in two hours intervals for 22 h. Each experiment is repeated to check the reproducibility. The conversion of N_2O (R_{N2O}) is calculated using the equation 1 where x^0_{N2O} is the initial mole fraction of N_2O and x_{N2O} is the mole fraction at different times during the photocatalytic reaction.

$$R_{N2O} = \frac{x^0_{N2O} - x_{N2O}}{x^0_{N2O}} \quad (1)$$

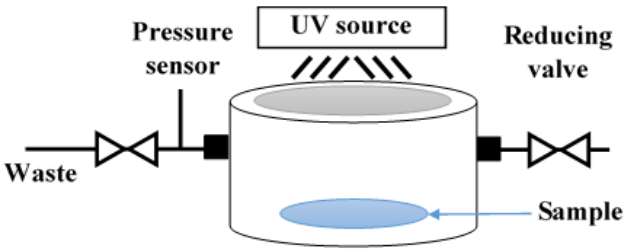

Figure 1. Scheme of the photo-reactor used to decompose N_2O gas.

2.3 Degradation of SMX in water

Concerning the photocatalytic degradation of SMX solution (50 µM), the photocatalytic layers are placed at the bottom of home-made photo-reactor equipped of four UVA lamps at the top (Sylvania F15W/350BL; 1.9 mW cm^{-2} in the range 290-400 nm). Prior to turn on the lamps, the initial pH of SMX solution is adjusted at 7 using $HClO_4$ and NaOH. The photocatalytic degradation is performed under constant air bubbling for 4 h and 500 µL is sampled out every 30 min (filtration through 0.45 µm PTFE filter and quenching into 100 µL methanol). The concentration of SMX is analyzed by HPLC (Shimadzu Nexera XR LC-20AD) equipped with a C18 column (Agilent, EC 250/4.6 nucleodur 100/5). The mobile phase is a mixture of MeOH/H_2O in gradient mode from 40:60 (v/v) to 95:5 (v/v) which is achieved in 10 min. The detection wavelength of SMX is fixed at 268 nm.

In addition, to highlight the significance of the present study for potential industrial application, the degradation of SMX is performed in secondary effluent of municipal wastewater treatment plants collected in Clermont-Ferrand, France. Prior to use it as wastewater matrix, it is filtered through 0.45 µm PTFE membrane and further analyzed by total organic analysis (Shimadzu, TOC-L) and ionic chromatography (Thermo Scientific, ICS 5000). The data are presented in Table 1.

Table 1. Concentration of inorganic ions and inorganic and organic carbon.

Species	Concentration (mg L^{-1})
Cl^-	100
NO_3^-	59
SO_4^{2-}	53
PO_4^{3-}	< LOD [1]
Na^+	131
NH_4^+	4
K^+	40
Mg^{2+}	9
Ca^{2+}	25
Inorganic C	47
Organic C	7

[1] Under the Limit Of Detection.

The identification of SMX transformation by-products is obtained by ultra-high performance liquid chromatography (UHPLC) coupled with high-resolution mass spectrometry (HRMS) performed on an Orbitrap Q-Exactive (Thermo scientific). The column is a Phenomenex Kinetex C18 (1.7µm × 100 Å; 100 × 2.1mm) and the temperature is set at 30 °C. The initial gradient is 5% ACN and 95% water acidified with 1% formic acid, followed by a linear gradient to 99% ACN within 8.5 min and kept constant during 1 min. The flow rate is 0.45 mL min^{-1} and the injection volume is 5 µL. Ionization is set to 3.2 kV (ESI+) and 3.0 kV (ESI-).

3. Results and Discussion

3.1 Structural and optical properties of photocatalysts

The XRD patterns (Figure S1) of the F20, F40, F60, F80 and SG samples match with the anatase phase of TiO_2 (ICDD card no. 03-065-5714) as reported in our previous works [20,34]. Very weak diffractions of TiO_2 anatase phase are also confirmed in SG sample, where textured silicon wafer was used as the substrate. Therefore, additional diffractions of the textured silicon wafers correspond to the K_{beta}, L_{alpha1} and L_{alpha2} lines of Si (111) along with impurities. It is worth noting the diffractions from metallic Ti in the TNT layers since it is the underlying substrate of self-organized and highly oriented TiO_2 nanotubes. In addition, the F0 sample only exhibit metallic Ti diffraction (ICDD card no. 00-044-1294) although an ultra-thin layer of TiO_2 (several nanometers) might be present due to surface oxidation.

The SEM pictures (Figure 2) show that the photocatalysts possess different surface morphologies. The surface of the F0 sample exhibit typical morphology of Ti i.e., a dense structure of microcrystals (Figure 2a). As the anodization voltage increases from 20 to 80 V, a porous nanostructure is observed (Figure 2b-e). The F20 sample exhibit clear nanotubular morphology of self-organized and highly-ordered TNT layer. However, the surface of the TNT in F40 sample starts to be destroyed. In F60 and F80 samples, the nanotubular morphology disappears and a porous nanostructure is formed instead. Indeed, in F60 sample, the nanostructure is composed of reminiscent nanotube while in F80 sample, a sponge-like nanostructure is formed due to the high voltage, thus supporting the complete dissolution of the nanotubes. Concerning the SG sample, the surface morphology is dense due to the nanoparticulated structure (Figure 2f) [35]. The thickness of the anodized samples is about 2 µm while the SG exhibit a thickness of about 400 nm (Figure S2) [34].

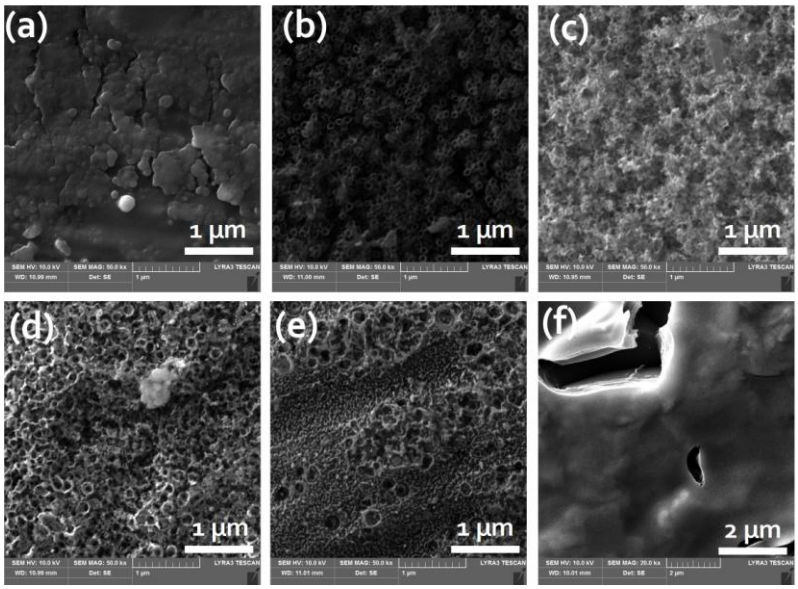

Figure 2. SEM pictures of (a) F0, (b) F20, (c) F40, (d) F60, (e) F80 and (f) SG.

Concerning the optical properties, the Tauc's plot (Figure 3) exhibits that the samples showing TNT morphology i.e., F20 and F40 possess the strongest light absorption along with E_g of about 3.3 eV. For porous nanostructures like F60 and F80 samples, light absorption decreases while the E_g is about 3.4 eV. For the SG sample, light absorption is weaker due to the thickness which is approx. 5 times thinner than anodized samples. In addition, the F0 sample which is essentially composed of metallic Ti exhibit slight absorption in UVA due to the upper oxidized layer.

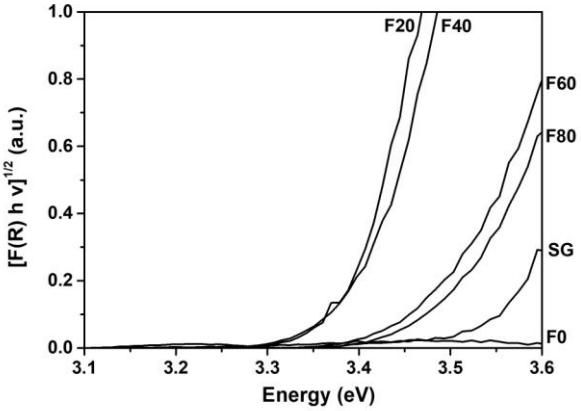

Figure 3. UV-visible DRS of the TiO_2 nanostructures.

3.2 N_2O reduction experiments

The ability of the TiO_2 photocatalysts prepared by two different methods (electrochemical anodization and sol-gel deposition) to reduce nitrous oxide under UVA light is investigated (Figure 4). It is worth noting there is no reference in the literature about the testing of photocatalytic decomposition of N_2O with the use of TiO_2 nanostructure prepared by electrochemical anodization, thus highlighting the significance of the present work.

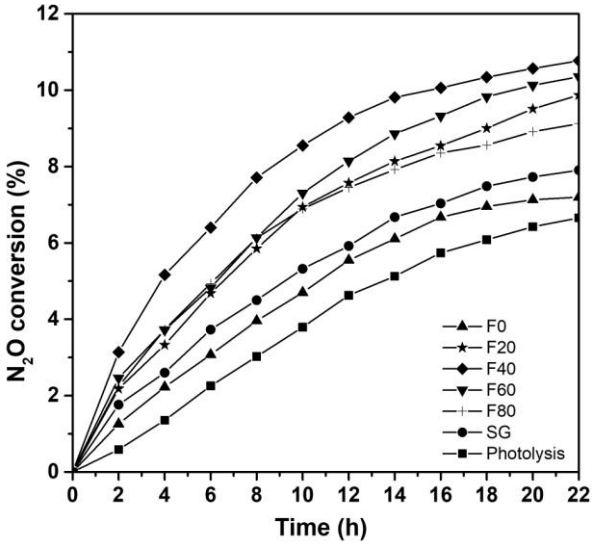

Figure 4. N_2O gas conversion under UVA light.

From the Figure 4, it is clear that N_2O conversion which occurs during photocatalytic reactions is significantly higher than direct photolysis (i.e., without photocatalyst). Comparing the different photocatalysts, the highest N_2O conversion is achieved using samples prepared by electrochemical anodization, especially F40 sample showing nanotubular morphology. Indeed, such a TNT layer can convert about 10% of N_2O after 22 h UVA irradiation. The lowest photocatalytic activities are observed for F0 and SG samples with a conversion about 7.2% and 7.9%, respectively. That is due to two main reasons which are supported by SEM analysis (Figure 2): (i) these samples exhibit significantly lower specific surface area compared to nanoporous F20, F40, F60 and F80 and (ii) their thickness is also smaller. Nevertheless, both of this poorly photoactive samples present a higher N_2O conversion than simple photolysis (6.6%).

3.3 Degradation of SMX

The degradation curves of SMX using the samples prepared by electrochemical anodization and sol-gel method are presented in Figure 5. Globally, similar trend is observed between N_2O reduction and SMX oxidation since the best samples are F20 and F40, i.e. samples with nanotubular morphology. This fact highlights the versatility of anodic TiO_2 nanotube layers. The degradation extent of SMX after 4 h UVA irradiation reaches 65% and 62% for in the presence of F20 and F40, respectively. The degradation extent decreases to 52% using F60, since the structure is composed of reminiscent nanotubes. The efficiency of the other samples is relatively poor due to the absence of nanotubular morphology. In other words, the number of catalytic sites and the lifetime of charge carriers is probably significantly reduced. The TOC analysis corroborates the degradation curves. Indeed, for F20, F40 and F60, the mineralization extent after 4 h UVA irradiation reaches 11%, 8% and 3%, respectively, while for the other samples, no mineralization takes place. The potential application of anodic TiO_2 layer in water treatment is performed by the degradation of SMX in secondary effluents of wastewater treatment plants (Figure S3). The degradation efficiency decreases from 65 to 45% due to the negative effects of the wastewater matrix, i.e. the dissolved organic matter that plays the role of ROS scavenger. However, the degradation efficiency is still considered to be satisfactory.

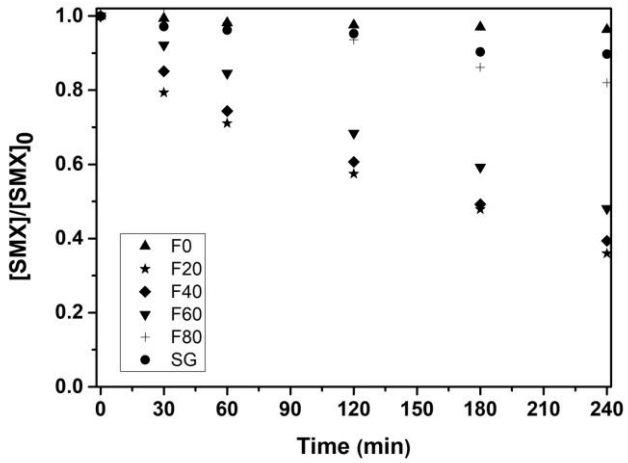

Figure 5. Degradation of SMX under UVA light.

In order to get better insights into the degradation mechanism using F20, the SMX degradation by-products are identified using LC-MS. The transformation products of SMX are presented in Table S1. The initial SMX molecule displayed a peak at $[M+H]^+$ = 254.0592 and a sodium adduct $[M+Na]^+$ = 276.0410 and $[M-H]^-$ = 252.0441. Different degradation pathways are proposed considering the identification of SMX by-products (Figure 6). The formation of P1 occurs through the photo-isomerization of the isoxazole ring which is also the dominant pathway in the degradation of SMX under UV-mediated degradation [36]. Electrophilic reaction on the aromatic ring leads to the formation of hydroxylated (P2) and dihydroxylated (P3) products while oxidation of the double bond at the isoxazole ring produced P4. The cleavage of sulfonamide bond by the hydroxyl radical leads to the formation of 3-amino-5-methylisoxazole (P5) and sulfanilic acid (P4). Isoxazole ring rearrangement leads to the formation of P7 that can be further oxidized on the amine ring in the presence of hydroxyl radical leading to the formation of P7 and P8. The degradation mechanism confirms the predominant role of hydroxyl radicals.

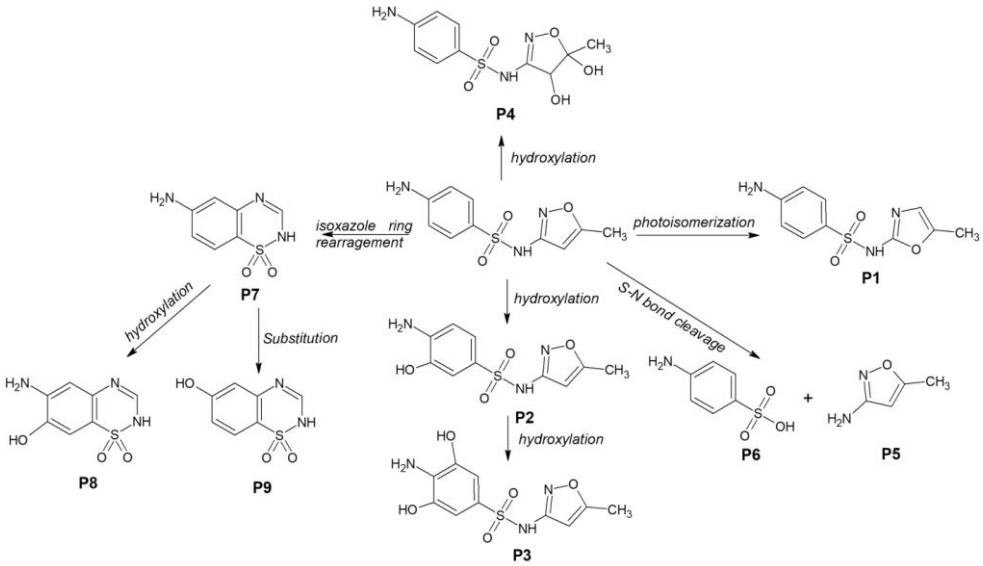

Figure 6. Proposed mechanism of SMX degradation under UVA light in the presence of anodic TiO_2 nanotube layer.

4. Conclusion

The preparation of different TiO_2 nanostructures including nanotube layers and thin films has been performed using electrochemical anodization and sol-gel method, respectively. Their performance in versatile photocatalytic applications has been assessed by investigating their ability to degrade gaseous and aqueous pollutants under UVA light i.e. N_2O and sulfamethoxazole. The best samples in both the photocatalytic reactions are those showing a nanotubular morphology (F20 and F40) probably due to their high specific surface area and excellent charge carriers transport, compared to others samples (F0, F60, F80 and SG) that show non-ordered and less porous nanostructures. In addition, the degradation mechanism of sulfamethoxazole has been proposed and has highlighted the crucial role of hydroxyl radicals. This work is significant since it proves the photocatalytic versatility of anodic TiO_2 nanotube layers in different applications like the remediation of air and water. Indeed, the degradation of sulfamethoxazole has been tested in secondary effluents from wastewater treatment plant, and has confirmed the efficiency of the anodic TiO_2 nanotube layers.

Supplementary Materials: The following supporting information can be downloaded at: www.mdpi.com/xxx/s1, Figure S1: XRD of the TiO_2 nanostructures; Figure S2: SEM picture of the thickness of SG; Figure S3: Degradation of SMX in secondary effluents of wastewater treatment plant using F20 under UVA light; Table S1: LC-MS data of SMX degradation by-products.

Author Contributions: Conceptualization, O.M.; methodology, M.S., M.B and O.M.; formal analysis, M.S., S.G., A.M., M.B. and O.M.; investigation, M.S., S.G., A.M.; data curation, M.S. A.M, and M.B.; writing—original draft preparation, O.M., M.S., S.G., M.M.; writing—review and editing, O.M. and M.B.; supervision, O.M.and G.M.; funding acquisition, O.M., M.S., and G.S.; All authors have read and agreed to the published version of the manuscript.

Funding: This work was co-financed by the Slovak Research and Development Agency (under the contracts No. APVV-21-0039 and No. APVV-21-0053), the Scientific Grant Agency of the Ministry of Education, Science, Research and Sport of the Slovak republic (through the VEGA project No. 1/0062/22) and the Operation Program of Integrated Infrastructure supported by the ERDF for the project "Upscale of Comenius University Capacities and Competence in Research, Development and Innovation" (ITMS 2014+: 313021BUZ3). Sridhar Gowrisankaran also acknowledges the financial support provided by the Comenius University Bratislava through the project No. UK/180/2022. Experimental results were accomplished by using Large Research Infrastructure ENREGAT supported by the Ministry of Education, Youth and Sports of the Czech Republic under project No. LM2018098.

Institutional Review Board Statement: Not applicable.

Informed Consent Statement: Not applicable.

Data Availability Statement: Not applicable.

Acknowledgments: The authors acknowledge Guillaume Voyard of the Institute of Chemistry of Clermont-Ferrand for the technical support provided for the HPLC analysis.

Conflicts of Interest: The authors declare no conflict of interest. The funders had no role in the design of the study; in the collection, analyses, or interpretation of data; in the writing of the manuscript; or in the decision to publish the results.

References

1. Hashimoto, K.; Irie, H.; Fujishima, A. TiO_2 Photocatalysis: A Historical Overview and Future Prospects. *Japanese J. Appl. Physics, Part 1 Regul. Pap. Short Notes Rev. Pap.* **2005**, *44*, 8269–8285, doi:10.1143/JJAP.44.8269.
2. Schneider, J.; Matsuoka, M.; Takeuchi, M.; Zhang, J.; Horiuchi, Y.; Anpo, M.; Bahnemann, D.W. Schneider et Al. - 2014 - Understanding TiO_2 Photocatalysis Mechanisms and Materials *Chem. Rev.* **2014**, *114*, 9919–9986.
3. Moradeeya, P.G.; Sharma, A.; Kumar, M.A.; Basha, S. Titanium Dioxide Based Nanocomposites – Current Trends and Emerging Strategies for the Photocatalytic Degradation of Ruinous Environmental Pollutants. *Environ. Res.* **2022**, *204*,

299 112384, doi:10.1016/j.envres.2021.112384.
300 4. Wu, M.J.; Bak, T.; O'Doherty, P.J.; Moffitt, M.C.; Nowotny, J.; Bailey, T.D.; Kersaitis, C. Photocatalysis of Titanium Dioxide
301 for Water Disinfection: Challenges and Future Perspectives. *Int. J. Photochem.* **2014**, *2014*, 1–9, doi:10.1155/2014/973484.
302 5. Kumar, S.G.; Devi, L.G. Review on Modified TiO_2 Photocatalysis under UV/Visible Light: Selected Results and Related
303 Mechanisms on Interfacial Charge Carrier Transfer Dynamics. *J. Phys. Chem. A* **2011**, *115*, 13211–13241,
304 doi:10.1021/jp204364a.
305 6. Lan, Y.; Lu, Y.; Ren, Z. Mini Review on Photocatalysis of Titanium Dioxide Nanoparticles and Their Solar Applications.
306 *Nano Energy* **2013**, *2*, 1031–1045, doi:10.1016/j.nanoen.2013.04.002.
307 7. Motola, M.; Dworniczek, E.; Satrapinskyy, L.; Chodaczek, G.; Grzesiak, J.; Gregor, M.; Plecenik, T.; Nowicka, J.; Plesch, G.
308 UV Light-Induced Photocatalytic, Antimicrobial, and Antibiofilm Performance of Anodic TiO_2 Nanotube Layers Prepared
309 on Titanium Mesh and Ti Sputtered on Silicon. *Chem. Pap.* **2019**, *73*, 1163–1172, doi:10.1007/s11696-018-0667-4.
310 8. Yemmireddy, V.K.; Hung, Y.C. Using Photocatalyst Metal Oxides as Antimicrobial Surface Coatings to Ensure Food
311 Safety—Opportunities and Challenges. *Compr. Rev. Food Sci. Food Saf.* **2017**, *16*, 617–631, doi:10.1111/1541-4337.12267.
312 9. Fagan, R.; McCormack, D.E.; Dionysiou, D.D.; Pillai, S.C. A Review of Solar and Visible Light Active TiO_2 Photocatalysis
313 for Treating Bacteria, Cyanotoxins and Contaminants of Emerging Concern. *Mater. Sci. Semicond. Process.* **2016**, *42*, 2–14,
314 doi:10.1016/j.mssp.2015.07.052.
315 10. Motola, M.; Zazpe, R.; Hromadko, L.; Prikryl, J.; Cicmancova, V.; Rodriguez-Pereira, J.; Sopha, H.; Macak, J.M. Anodic TiO_2
316 Nanotube Walls Reconstructed: Inner Wall Replaced by ALD TiO_2 Coating. *Appl. Surf. Sci.* **2021**, *549*,
317 doi:10.1016/j.apsusc.2021.149306.
318 11. Macak, J.M.; Zlamal, M.; Krysa, J.; Schmuki, P. Self-Organized TiO2 Nanotube Layers as Highly Efficient Photocatalysts.
319 *Small* **2007**, *3*, 300–304, doi:10.1002/smll.200600426.
320 12. Kubacka, A.; Diez, M.S.; Rojo, D.; Bargiela, R.; Ciordia, S.; Zapico, I.; Albar, J.P.; Barbas, C.; Martins Dos Santos, V.A.P.;
321 Fernández-García, M.; et al. Understanding the Antimicrobial Mechanism of TiO_2 -Based Nanocomposite Films in a
322 Pathogenic Bacterium. *Sci. Rep.* **2014**, *4*, 1–9, doi:10.1038/srep04134.
323 13. Macák, J.M.; Tsuchiya, H.; Ghicov, A.; Schmuki, P. Dye-Sensitized Anodic TiO_2 Nanotubes. *Electrochem. commun.* **2005**, *7*,
324 1133–1137, doi:10.1016/j.elecom.2005.08.013.
325 14. Regonini, D.; Chen, G.; Leach, C.; Clemens, F.J. Comparison of Photoelectrochemical Properties of TiO_2 Nanotubes and
326 Sol-Gel. *Electrochim. Acta* **2016**, *213*, 31–36, doi:10.1016/j.electacta.2016.07.097.
327 15. Beranek, R.; Tsuchiya, H.; Sugishima, T.; Macak, J.M.; Taveira, L.; Fujimoto, S.; Kisch, H.; Schmuki, P. Enhancement and
328 Limits of the Photoelectrochemical Response from Anodic TiO_2 Nanotubes. *Appl. Phys. Lett.* **2005**, *87*, 1–3,
329 doi:10.1063/1.2140085.
330 16. Thompson, T.L.; Yates, J.T. Surface Science Studies of the Photoactivation of TiO_2 - New Photochemical Processes. *Chem.*
331 *Rev.* **2006**, *106*, 4428–4453, doi:10.1021/cr050172k.
332 17. Lee, K.; Mazare, A.; Schmuki, P. One-Dimensional Titanium Dioxide Nanomaterials : Nanotubes. **2014**.
333 18. Roy, P.; Berger, S.; Schmuki, P. TiO_2 Nanotubes: Synthesis and Applications. *Angew. Chemie - Int. Ed.* **2011**, *50*, 2904–2939,
334 doi:10.1002/anie.201001374.
335 19. Sopha, H.; Baudys, M.; Krbal, M.; Zazpe, R.; Prikryl, J.; Krysa, J.; Macak, J.M. Scaling up Anodic TiO_2 Nanotube Layers for
336 Gas Phase Photocatalysis. *Electrochem. commun.* **2018**, *97*, 91–95, doi:10.1016/j.elecom.2018.10.025.
337 20. Hanif, M.B.; Sihor, M.; Liapun, V.; Makarov, H.; Monfort, O.; Motola, M. Porous vs. Nanotubular Anodic TiO_2: Does the
338 Morphology Really Matters for the Photodegradation of Caffeine? *Coatings* **2022**, *12*, 1–12, doi:10.3390/coatings12071002.
339 21. Crini, G.; Lichtfouse, E. Advantages and Disadvantages of Techniques Used for Wastewater Treatment. *Environ. Chem. Lett.*
340 **2019**, *17*, 145–155, doi:10.1007/s10311-018-0785-9.

22. Devipriya, S.; Yesodharan, S. Photocatalytic Degradation of Pesticide Contaminants in Water. *Sol. Energy Mater. Sol. Cells* **2005**, *86*, 309–348, doi:10.1016/j.solmat.2004.07.013.
23. Wilkinson, J.L.; Boxall, A.B.A.; Kolpin, D.W.; Leung, K.M.Y.; Lai, R.W.S.; Wong, D.; Ntchantcho, R.; Pizarro, J.; Mart, J.; Echeverr, S.; et al. Pharmaceutical Pollution of the World ' s Rivers. **2022**, *119*, 1–10, doi:10.1073/pnas.2113947119/-/DCSupplemental.Published.
24. Mackuľak, T.; Černanský, S.; Fehér, M.; Birošová, L.; Gál, M. Pharmaceuticals, Drugs, and Resistant Microorganisms — Environmental Impact on Population Health. *Curr. Opin. Environ. Sci. Heal.* **2019**, *9*, 40–48, doi:10.1016/j.coesh.2019.04.002.
25. Decision 2020/1161/EU Commision Implementing Decision (EU) 2020/1161-4 August 2020-Establishing a Watch List of Substances for Union-Wide Monitoring in the Field of Water Policy Pursuant to Directive 2008/105/EC of the European Parliament and of the Council. *Off. J. Eur. Union* **2020**, *257*, 32–35.
26. Ebitani, K.; Morokuma, M.; Kim, J.H.; Morikawa, A. Photocatalytic Decomposition of Nitrous Oxide on Cu Ion-Containing ZSM-5 Catalyst. *J. Catal.* **1993**, *141*, 725–728, doi:10.1006/jcat.1993.1177.
27. deRichter, R.; Caillol, S. Fighting Global Warming: The Potential of Photocatalysis against CO_2, CH_4, N_2O, CFCs, Tropospheric O_3, BC and Other Major Contributors to Climate Change. *J. Photochem. Photobiol. C Photochem. Rev.* **2011**, *12*, 1–19, doi:10.1016/j.jphotochemrev.2011.05.002.
28. Sano, T.; Negishi, N.; Mas, D.; Takeuchi, K. Photocatalytic Decomposition of N_2O on Highly Dispersed Ag^+ Ions on TiO_2 Prepared by Photodeposition. *J. Catal.* **2000**, *194*, 71–79, doi:10.1006/jcat.2000.2915.
29. Obalová, L.; Reli, M.; Lang, J.; Matějka, V.; Kukutschová, J.; Lacný, Z.; Kočí, K. Photocatalytic Decomposition of Nitrous Oxide Using TiO_2 and Ag-TiO_2 Nanocomposite Thin Films. *Catal. Today* **2013**, *209*, 170–175, doi:10.1016/j.cattod.2012.11.012.
30. Kočí, K.; Krejčíková, S.; Šolcová, O.; Obalová, L. Photocatalytic Decomposition of N_2O on Ag-TiO_2. *Catal. Today* **2012**, *191*, 134–137, doi:10.1016/j.cattod.2012.01.021.
31. Matějová, L.; Polách, L.; Lang, J.; Šihor, M.; Reli, M.; Brunátová, T.; Daniš, S.; Peikertová, P.; Troppová, I.; Kočí, K. Novel TiO_2 Prepared from Titanyl Sulphate by Using Pressurized Water Processing and Its Photocatalytic Activity Evaluation. *Mater. Res. Bull.* **2017**, *95*, 30–46, doi:10.1016/j.materresbull.2017.07.010.
32. Kočí, K.; Reli, M.; Troppová, I.; Šihor, M.; Kupková, J.; Kustrowski, P.; Praus, P. Photocatalytic Decomposition of N_2O over TiO_2/g-C_3N_4 Photocatalysts Heterojunction. *Appl. Surf. Sci.* **2017**, *396*, 1685–1695, doi:10.1016/j.apsusc.2016.11.242.
33. Yuan, R.; Wang, M.; Liao, L.; Hu, W.; Liu, Z.; Liu, Z.; Guo, L.; Li, K.; Cui, Y.; Lin, F.; et al. 100% N_2O Inhibition in Photocatalytic NOx Reduction by Carbon Particles over Bi_2WO_6/TiO_2 Z-Scheme Heterojunctions. *Chem. Eng. J.* **2023**, *453*, 139892, doi:10.1016/j.cej.2022.139892.
34. Sihor, M.; Hanif, M.B.; Thirunavukkarasu, G.K.; Liapun, V.; Edelmannova, M.F.; Roch, T.; Satrapinskyy, L.; Plecník, T.; Rauf, S.; Hensel, K.; et al. Anodization of Large Area Ti: A Versatile Material for Caffeine Photodegradation and Hydrogen Production. *Catal. Sci. Technol.* **2022**, *12*, 5045–5052, doi:10.1039/d2cy00593j.
35. Monfort, O.; Roch, T.; Gregor, M.; Satrapinskyy, L.; Raptis, D.; Lianos, P.; Plesch, G. Photooxidative Properties of Various $BiVO_4$/TiO_2 Layered Composite Films and Study of Their Photocatalytic Mechanism in Pollutant Degradation. *J. Environ. Chem. Eng.* **2017**, *5*, 5143–5149, doi:10.1016/j.jece.2017.09.050.
36. Ao, X.; Liu, W.; Sun, W.; Yang, C.; Lu, Z.; Li, C. Mechanisms and Toxicity Evaluation of the Degradation of Sulfamethoxazole by MPUV/PMS Process. *Chemosphere* **2018**, *212*, 365–375, doi:10.1016/j.chemosphere.2018.08.031.